Quantum well states with nonvanishing parallel momentum in Cu/Co/Cu(100)

P. Kloth, M. Wenderoth,* P. Willke, H. Prüser,† and R. G. Ulbrich
IV Physikalisches Institut, Georg-August-Universität Göttingen, Friedrich-Hund-Platz 1, 37077 Göttingen, Germany
(Received 2 July 2013; revised manuscript received 21 February 2014; published 10 March 2014)

Using low-temperature scanning tunneling spectroscopy we study quantum well states in the topmost copper layer of a Cu/Co/Cu(100) system above the Fermi energy. The emergence and the energetic positions of QWSs within this layer crucially depend on the interface quality tailored by the sample preparation method. Samples deposited at room temperature show a rough interface and lead to the well-known QWSs with only a momentum perpendicular to the interface. Atomically smooth interfaces for samples grown at 80 K exhibit states caused by stationary points with a large nonvanishing parallel momentum. Simulations taking into account the different band structures allow QWSs to be modeled from both stationary points and an identification of a crossover between bound and resonance states.

DOI: 10.1103/PhysRevB.89.125412 PACS number(s): 75.75.Cd, 68.35.Ct, 68.37.Ef, 73.21.Fg

I. INTRODUCTION

Interlayer exchange coupling (IEC) in magnetic/nonmagnetic quantum well structures has attracted great interest in the last two decades. Since its first discovery [1–3], IEC has stimulated fundamental studies and triggered novel applications in sensor and storage technology. Experiments using the magneto-optical Kerr effect (MOKE) have shown a characteristic oscillatory behavior from ferro- to antiferromagnetic coupling as a function of the spacer thickness [4,5]. Photoemission spectroscopy (PES) has revealed that the coupling is mediated by quantum well states (QWSs) in the nonmagnetic layer [6,7]. Moreover, theoretical [8–11] and experimental [12–17] studies have proven that more than one coupling period for the IEC can exist in sandwich structures. QWSs are formed by stationary points on the Fermi surface. Each coupling period is directly linked to one stationary point of the material forming the quantum well. The visibility in experiments of a specific coupling period is very sensitive to the preparation process [13–15]. In particular, the structural properties in terms of roughness at the interfaces play an important role. It is an open question what kind of roughness causes this selection of QWSs. Disorder due to a high concentration of steps and islands and the diffusive intermixing of the materials at the interface have been discussed [9,13,14].

In this article we present a detailed scanning tunneling microscopy (STM) and scanning tunneling spectrosocopy (STS) investigation of the interplay between the interface structure and the resulting electronic properties of a layered system made of magnetic Co and nonmagnetic Cu(100) [see Fig. 1(a)] [18–21]. The small lattice mismatch of the two materials in the fcc configuration provides good epitaxial growth. Nevertheless, thin film deposition of this system is a complex process [22–27]. Segregation and diffusion cause roughening of the interfaces. We conduct a detailed growth analysis by investigating the surface of each layer for different growth regimes with the help of STM topographies. At the same time the spectroscopic mode allows us to characterize the electronic properties of our structures on the nanometer scale.

Crucial for the QWSs are the electronic properties of the host materials. These include the band structure of Cu, which defines the dispersive behavior and the possible stationary points for the QWSs. Matching the confined states in the Cu well at the interface involves the band structure of Co. Figure 1(b) shows isoenergy surfaces of Cu and spin-down Co. Two different stationary points in the (100) direction of Cu exist, one at the belly and one at the neck of the surface. These points are characterized by a vanishing group velocity in the $k_{\parallel}$ direction and thus dominate the local density of states (LDOS).

II. GROWTH ANALYSIS

The main idea of this study is to tailor the interface roughness of the Cu/Co/Cu(100) system using different growth conditions. Probing these structures on a nanometer scale allows investigation of the influence of the interface on QWSs in a controlled manner. We start with a commercial Cu(100) single crystal, which is cleaned by several cycles of sputtering with argon bombardment and subsequent annealing steps. Cu and Co layers are deposited by electron beam evaporation at a base pressure below 10^{-10} mbar, resulting in epitaxially grown films. The evaporation rate is 1 monolayer (ML) per minute. A precise calibration allows a controlled deposition of films in the ML range. Further low-energy electron diffraction studies assured the epitaxial growth of each layer. The sample analysis is done by a home-built STM, operating in ultrahigh-vacuum conditions at 6 K.

We have grown two variants of the sandwich system. (i) Room temperature (RT): After the deposition of 10 ML of Co the film is annealed with electron beam heating from the back side of the sample at 450 K for 5 min before the Cu film with a thickness of 12 ML is prepared. (ii) Low temperature (LT) at 80 K: Again the 10 ML of Co are subsequently annealed at 450 K for 5 min. After the nanostructure is cooled down to 80 K again, Cu films of 9 and 12 ML were deposited, respectively.

As illustrated in Fig. 2 the heterostructures grown at RT [Figs. 2(a)–2(d)] differ considerably from the layered systems grown at LT [Figs. 2(e)–2(h)]. In Fig. 2(a), for the

*wenderoth@ph4.physik.uni-goettingen.de
†Present address: London Centre for Nanotechnology, University College London, United Kingdom.

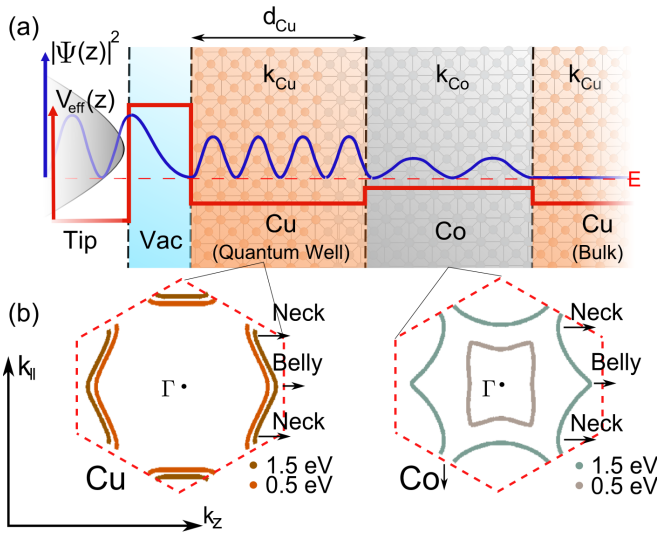

FIG. 1. (Color online) (a) A sketch of the Cu/Co/Cu(100) layered system including the STM tip in tunneling contact. The red line sketches an effective potential $V_{\text{eff}}(z)$ that was derived from the transfer matrix method and the Cu/Co band structure. The blue line shows the wave function of a QWS. (b) Cross sections along the (011) direction of two isoenergetic surfaces at 0.5 and 1.5 eV above the Fermi energy of Cu (left) and spin-down Co (right). The arrows indicate the two stationary points on this isoenergetic surface in the (100) direction.

RT-grown sample the Co film shows a layer-by-layer type of growth [22,23]. Annealing causes a smoothing of the morphology as shown in Fig. 2(b). The topmost Cu layer is shown in Fig. 2(c) and reveals contamination with Co atoms in Fig. 2(d) as dark rounded contrasts. This probably results from segregation during deposition [25–27]. For the LT preparation the low thermal energy at the surface causes a rough growth for the Co layer with a great amount of small islands [Fig. 2(e)]. The additional annealing step produces a flatter surface than in the RT case, shown in Fig. 2(f). But as a trade-off for this smoothness the layer shows a higher concentration of stacking faults (10 screw dislocations on 100×100 nm^2) induced by the small mismatch of the lattice constants of Cu and Co. The subsequent Cu surface is flat on a length scale of several tenths of nanometers [Fig. 2(g)]. This indicates a high mobility of the Cu atoms, even at LT. A high-resolution topography of the surface in Fig. 2(h) shows again Co defects. In comparison to the RT preparation the relative concentration of Co atoms in the first layer is reduced about nearly five times. Since the intermixing is mainly driven by the segregation during the growth [26,27] and not by additional diffusion afterwards, we expect also a less rough Co/Cu interface. In summary, RT and LT preparation result in layered structures with similar concentrations of steps and islands. In the case of LT growth the atomic intermixing can be reduced considerably.

III. ELECTRONIC ANALYSIS

The electronic analysis of these two morphologically different samples is done by STS. Using the tip as a local probe for current injection one can identify the presence of QWSs in the Cu layer as a change in the LDOS. The numerical derivative

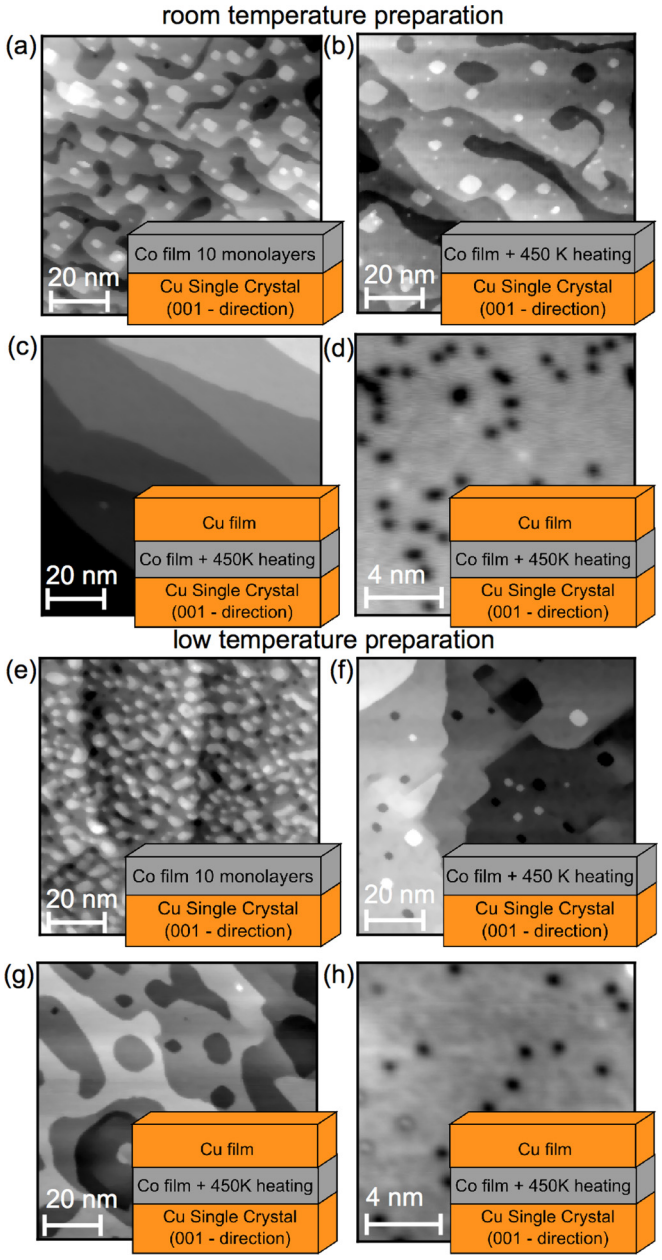

FIG. 2. (Color online) STM topographies after different preparation steps for the RT and LT growth: (a), (e) 10 ML of Co on a Cu(100) single crystal. (b), (f) The same surface after a 5 min annealing step at 450 K. (c), (g) After 12 ML of Cu no additional annealing is needed [1 V at 0.1 nA (RT)/0.5 nA (80 K)]. (d), (h) A more detailed view of the Cu layer reveals a segregation process of Co into the Cu film at room temperature. The same is observed for deposition at low temperature but up to five times less than in the room-temperature case [30 mV (RT)/10 mV at 1 nA (80 K)].

of the local $I(V)$ curves offers direct access to the LDOS. This approach gives a connection between the interface properties and the corresponding electronic features. Figure 3(a) shows two raw dI/dV curves taken on a heterostructure grown at RT and on a bare Cu(100) crystal. In the case of the layered system the dI/dV curve shows steplike signatures due to the two-dimensional (2D) confinement whereas the differential conductivity for the bulk Cu(100) crystal is smooth

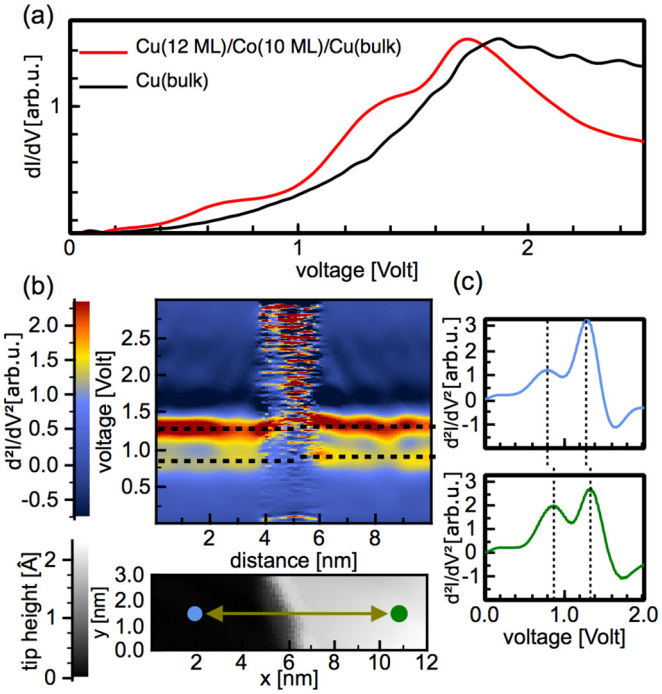

FIG. 3. (Color online) Electronic analysis of the QWSs. (a) Raw tunneling spectra of a Cu(100) bulk single crystal (black line) and of the Cu/Co/Cu heterostructure grown at RT (red line) (−3 V at 2 nA). (b) A section of the derivative of the differential conductivity over a monatomic step, shown in the topography at the bottom for the system grown at LT. (c) Two single spectra of the second derivative of the current, each taken at one of the two dots in the topography (3 V at 3 nA).

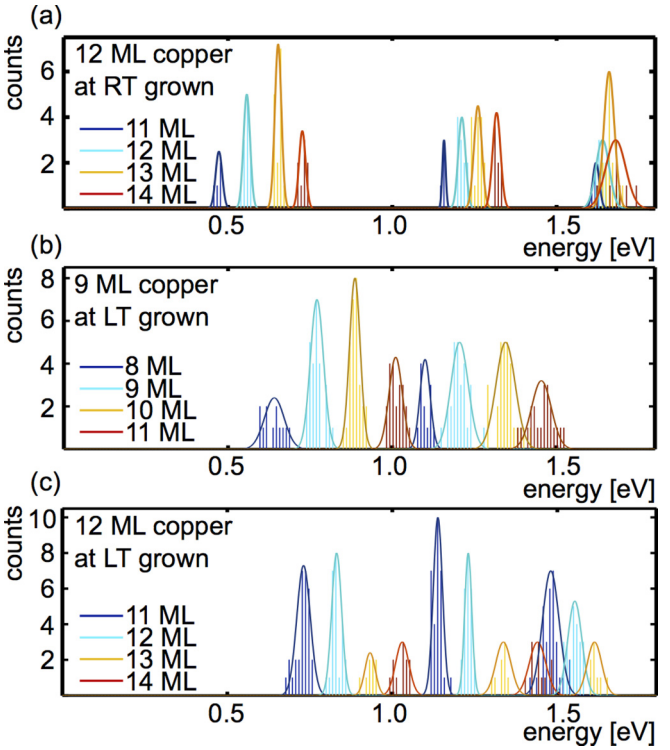

FIG. 4. (Color online) Statistical analysis of the energetic position of the QWS signatures. The energies accumulate to certain values, which are then attributed to the numbers of monolayers around the calibrated thickness from the evaporation. (a) and (c) show the analysis for the 12 ML copper grown at RT and LT, respectively, and (b) the analysis of the 9 ML film of copper prepared at LT.

and featureless. The depletion of the LDOS at 1.8 eV is caused by the top of the *sp* band at the *X* point in the band structure.

For a thickness-dependent analysis the method of identification of the exact energetic position of each QWS has to be defined. We take the point of the highest slope at each step or the local maximum of the derivative of the differential conductivity. Figure 3(b) shows a spectroscopic section for the derivative of the differential conductivity over a single atomic step on the Cu film for the LT-prepared sample. This section visualizes the run of the QWS signatures color coded by changing the size of the confinement by 1 ML. One can see that the maxima, here in red, shift to higher energies for a thicker Cu film. This behavior can be better seen in two single spectra. One is taken on the lower terrace and the other is taken on the higher terrace in Fig. 3(c): The two maxima move up in energy for an increase of the thickness of the confinement.

Since the exact number of monolayers is locally not known, we extract the energetic positions of the QWSs for different-sized Cu layers in a statistical manner. Large-sized spectroscopic maps of the surface allow the evaluation of spectra for different thicknesses, as the prepared sample always exhibits a certain variation in the number of layers due to steps and islands. Figure 4 shows that especially in the lower-energy regions the signatures of the QWSs accumulate to distinct energies. Using the fact that each single spectrum contains three different signatures, we can transfer the ordering of the values in the lower regions to the values above 1.6 eV, where the accumulation points cannot be separated by the eye. Gaussian fits help to find the mean value of each accumulation point. Overall we can extract the QWS energies for four different thicknesses, which we then distribute along the nominal thickness coming from the gauge of the evaporator [28]. The result of this analysis is shown as circles in Fig. 5 for the sample prepared at RT and as triangles for the sample grown at LT. A comparison reveals a different dispersive behavior of the QWSs for the two preparation methods. Although in each case the eigenenergies of the quantized states evolve along three branches, the energetic positions clearly change.

IV. THEORETICAL MODELLING

A standard model to describe the thickness-dependent dispersion of QWSs is the widely used phase accumulation model (PAM) [19,29–32]. This model describes the wave function inside the well by including a dispersion of the stationary point on the Fermi surface and additional phase shifts at the interfaces. Using the dispersion at the belly, the results of the RT-grown sample can be reproduced by the PAM. The description of the values for the LT-grown samples fails based on using the dispersion of the neck region as well as the belly region [33]. Obviously the PAM cannot describe the phase matching of the QWSs in the neck region at the Cu/Co interface because of the complex band structure of Co

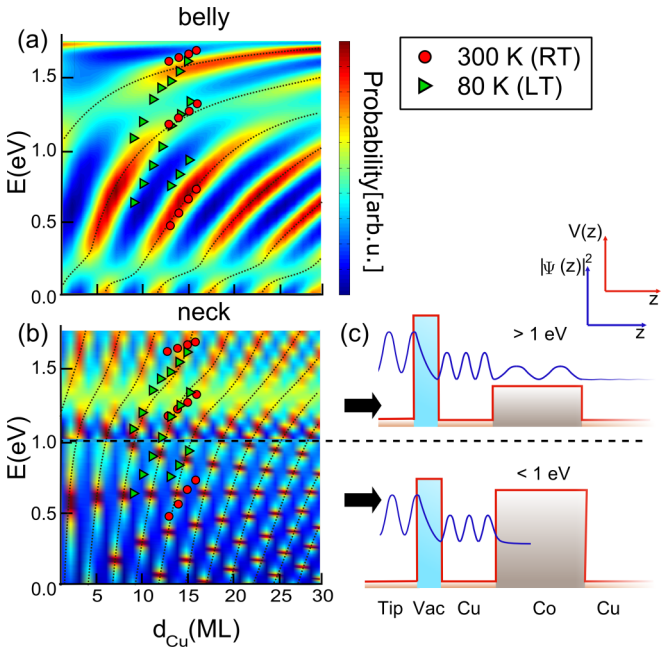

FIG. 5. (Color online) Comparison between experimental data and numerical results for (a) the belly states and (b) the neck states. The experimental results are plotted as circles for the RT-grown structure and as triangles for the LT-prepared sample, the numerically obtained probability of the electron to be found inside the Cu well is shown color coded (scaled logarithmically). The black lines are a guide to the eye for the respective dispersion branches. The values for the sample grown at RT fit the dispersion for the belly while the values for the LT-grown sample clearly fail. On the contrary, the latter match the dispersion for the neck states in (b). In (c) the schematic formation of the two kinds of QWSs for the energies in (b) is shown. Below 1 eV we obtain bound states; above that resonant transmitting states are possible.

in this energy range: Due to symmetry arguments only the sixth band for spin-down Co can couple to the QWSs in the Cu film [10,32]. This band has its lowest value at about 1 eV in the (100) direction at the neck of the Fermi surface – causing a band gap below this energy. In the picture of confined electron waves this results in a crossover from bound to resonant states [see Fig. 5(c)].

To describe this change from confined to resonant states we implement an advanced model taking into account (i) the band structure of Cu and Co and (ii) using the transfer matrix method (TMM) to simulate the propagation of electrons through the layered system. Previously, tight-binding calculations have been demonstrated to be a successful tool to describe a Co/Cu/Cu heterostructure [34]. Our ansatz is based on the empirical method introduced by Slater and Koster [35] using the parameters provided by Papaconstantopoulos [36]. It consists of a nine-dimensional basis containing one s, three p, and five d orbitals, and it takes into account up to second-nearest-neighbor interactions. Concerning the spin-polarized cobalt band structure, we used splitting energies for s, p, e_g, and t_{2g} orbitals obtained by fitting to spin-polarized data [37] as was done by Perez-Diaz and Munoz [38,39]. The copper band has been evaluated at the belly and the neck, the cobalt band at the points with the same $k_\parallel$ component as the corresponding copper value.

Concerning the boundary conditions at the interfaces, the wave functions and their derivatives are chosen to be continuous. The choice of the right boundary conditions is very subtle as well as important: Inclusion of other conditions such as, e.g., BenDaniel-Duke boundary conditions [40], which are often used to describe semiconductor quantum wells (including effective mass calculations), could not reproduce the experimental data. Nevertheless, the choice is in general not unique [41,42]. Following the approach by Kroemer and Zhu, our results support the idea that the interface in metallic layers behaves differently from that in semiconductors [43]. We substitute the band structure below the lower edge of the sixth band in Co by a constant potential barrier height of $E_U = 1.0$ eV for the neck [32]. To implement the potential landscape of our system we made a few assumptions and simplifications: The STM tip is made of wolfram, but for the sake of simplicity we use the same potential as for copper. This is justified by the fact that the effect of this layer for the formation of QWSs in the copper layer is negligible. The vacuum gap is set to 0.7 nm. The potential height of the vacuum gap is modeled by the work function of copper (4.4 eV). The algorithm for the QWSs is now straightforward: First, one calculates the energy-dependent Cu wave vector belonging to the respective QWSs. Second, the k_z vector for Co↓ with the same $k_{||}$ component is calculated to ensure momentum conservation. Finally, the transfer matrix algorithm is applied by solving the one-dimensional Schrödinger equation for a particle in a potential well system using the parameters mentioned above. The integrated probability density

$$P(E,d_{\mathrm{Cu}}) = \int_{\mathrm{well}} |\Psi_{\mathrm{Cu}}(z)|^2 dz$$

in the Cu layer, calculated as a function of energy and Cu layer thickness, can then be compared to the experimentally measured LDOS obtained by STM.

V. DISCUSSION

The results for the belly and the neck states for the Fermi surface of Cu can be found color coded and scaled logarithmically in Fig. 5. Although the TMM needs only k vectors in Cu and Co to calculate the probability density, we sketched an effective potential landscape for a single propagating electron in Fig. 5(c). Both the belly and the neck states reveal distinct lines that increase in energy for thicker Cu layers. Each of these branches corresponds to a certain number of nodes, and with this a certain number of half wavelengths of the related wave function inside the Cu well. One recognizes the different dispersion in the k_z direction at the neck as the resonant states become closer together for varying Cu layer thicknesses. At the Fermi energy the periodicity of these lines reproduces nicely the periodic behavior of the IEC with values of 5.7 and 2.6 ML [12,15]. Above the Fermi level the line of QWSs for the neck states has not been investigated yet. The crossover from bound states with a potential barrier to resonant states can be seen at 1 eV in Fig. 5(b). The phase shifts in energy in Figs. 5(a) and 5(b) are caused by resonant

states in the cobalt film. The results for the belly point of Cu in Fig. 5(a) are in good agreement with those of, e.g., [10].

Putting these results together with the experimental values we find good agreement for the dispersion at the belly with the samples prepared at room temperature (red circles). Accordingly, the LT-grown samples (green triangles) fit the states at the neck. Even more, they are able to confirm the crossover between bound and resonant QWSs experimentally. We conclude that these signatures are induced by QWSs of the neck region of the Fermi surface. These states dominate our tunneling signal and consequently the density of states in the Cu film. Even though the belly states always exist, they are not detected via spectroscopy for the LT-prepared sample. Theoretical results calculating the transmission probability of electron waves confirm the dominance for the neck states due to a high reflectivity at the Cu/Co interface [11]. But one has to be aware that the study considers QWSs only at the Fermi energy, while in our case this behavior seems to be still valid for higher energies. Picking up on the outcome of the growth analysis we conclude that a high concentration of segregated cobalt at the interfaces and not the presence of islands and steps causes the quenching of the short-period QWSs in the layered structure grown at RT. On the atomic scale our results show that $k_{\parallel}$ conversion is essential for confined states in these systems.

VI. SUMMARY

In conclusion we have shown the existence of QWSs with nonvanishing parallel momentum above the Fermi energy. The surface and interface roughness influence the formation of QWSs and can select the emergence of both belly and neck states. For the RT-prepared sample we can detect only the states at the belly point whereas for the layered films prepared at LT we observe (i) less intermixing and (ii) QWSs with dispersion of the stationary point at the neck. Our simulations model the experimental data and show that both resonant and bound states give rise to QWSs in the topmost copper layer.

[1] J. C. Bruyere, G. Clerc, O. Massenet, R. Montmory, L. Neel, D. Paccard, and A. Yelon, J. Appl. Phys. **36**, 944 (1965).
[2] P. Grünberg, R. Schreiber, Y. Pang, M. B. Brodsky, and H. Sowers, Phys. Rev. Lett. **57**, 2442 (1986).
[3] M. N. Baibich, J. M. Broto, A. Fert, F. Nguyen, Van Dau, F. Petroff, P. Etienne, G. Creuzet, A. Friederich, and J. Chazelas, Phys. Rev. Lett. **61**, 2472 (1988).
[4] P. Grünberg, S. Demokritov, A. Fuss, M. Vohl, and J. A. Wolf, J. Appl. Phys. **69**, 4789 (1991).
[5] W. Weber, A. Bischof, R. Allenspach, Ch. Würsch, C. H. Back and D. Pescia, Phys. Rev. Lett. **76**, 3424 (1996).
[6] J. E. Ortega and F. J. Himpsel, Phys. Rev. Lett. **69**, 844 (1992).
[7] Z. Q. Qiu, J. Pearson, and S. D. Bader, Phys. Rev. B **46**, 8195 (1992).
[8] P. Bruno and C. Chappert, Phys. Rev. Lett. **67**, 1602 (1991).
[9] M. D. Stiles, Phys. Rev. B **48**, 7238 (1993).
[10] P. Lang, L. Nordström, K. Wildberger, R. Zeller, P. H. Dederichs, and T. Hoshino, Phys. Rev. B **53**, 9092 (1996).
[11] M. D. Stiles, J. Magn. Magn. Mater. **200**, 322 (1999).
[12] M. T. Johnson, S. T. Purcell, N. W. E. McGee, R. Coehoorn, J. aan de Stegge, and W. Hoving, Phys. Rev. Lett. **68**, 2688 (1992).
[13] P. Segovia, E. G. Michel, and J. E. Ortega, Phys. Rev. Lett. **77**, 3455 (1996).
[14] R. Kläsges, D. Schmitz, C. Carbone, W. Eberhardt, P. Lang, R. Zeller, and P. H. Dederichs, Phys. Rev. B **57**, R696 (1998).
[15] C. Stamm, Ch. Würsch, S. Egger, and D. Pescia, J. Magn. Magn. Mater. **177–181**, 1279 (1998).
[16] R. Kawakami, E. Rotenberg, Hyuk J. Choi, Ernesto J. Escorcia-Aparicio, M. O. Bowen, J. H. Wolfe, E. Arenholz, Z. D. Zhang, N. V. Smith, and Z. Q. Qiu, Nature (London) **398**, 132 (1999).
[17] E. Rotenberg, Y. Z. Wu, J. M. An, M. A. Van Hove, A. Canning, L. W. Wang, and Z. Q. Qiu, Phys. Rev. B **73**, 075426 (2006).
[18] Ying-Shuang Fu, Shuai-Hua Ji, Xi Chen, Xu-Cun Ma, Rui Wu, Chen-Chen Wang, Wen-Hui Duan, Xiao-Hui Qiu, Bo Sun, Ping Zhang, Jin-Feng Jia, and Qi-Kun Xue, Phys. Rev. Lett. **99**, 256601 (2007).
[19] T. Uchihashi, J. Zhang, J. Kröger, and R. Berndt, Phys. Rev. B **78**, 033402 (2008).
[20] M. Becker and R. Berndt, Phys. Rev. B **81**, 205438 (2010).
[21] A. A. Khajetoorians, G. A. Fiete, and C.-K. Shih, Phys. Rev. B **81**, 041413(R) (2010).
[22] L. Gonzalez, R. Miranda, M. Salmeron, J. A. Verges, and F. Yndurain, Phys. Rev. B **24**, 3245 (1981).
[23] J. J. de Miguel, A. Cebollada, J. M. Gallego, and R. Miranda, J. Magn. Magn. Mater. **93**, 1 (1991).
[24] A. K. Schmid, D. Atlan, H. Itoh, B. Heinrich, T. Ichinokawa, and J. Kirschner, Phys. Rev. B **48**, 2855 (1993).
[25] J. Fassbender, R. Allenspach, and U. Drig, Surf. Sci. **383**, L742 (1997).
[26] T. Bernhard, R. Pfandzelter, M. Gruyters, and H. Winter, Surf. Sci. **575**, 154 (2005).
[27] T. Allmers and M. Donath, Surf. Sci. **605**, 1875 (2011).
[28] An error of at least 1 or 2 ML in the nominal thickness value has to be taken into account.
[29] P. Echenique and J. Pendry, J. Phys. C **11**, 2065 (1978).
[30] N. V. Smith, Phys. Rev. B **32**, 3549 (1985).
[31] J. E. Ortega, F. J. Himpsel, G. J. Mankey, and R. F. Willis, Phys. Rev. B **47**, 1540 (1993).
[32] Z. Q. Qiu and N. Smith, J. Phys.: Condens. Matter **14**, R169 (2002).
[33] The analysis has been done but is not shown in this article.
[34] S. Manna, P. L. Gastelois, M. Dabrowski, P. Kuswik, M. Cinal, M. Przybylski, and J. Kirschner, Phys. Rev. B **87**, 134401 (2013).
[35] J. Slater and G. Koster, Phys. Rev. **94**, 1498 (1954).
[36] D. A. Papaconstantopoulos, *Handbook of the Band Structure of Elemental Solids* (Plenum, New York, 1986).
[37] V. L. Moruzzi, J. F. Janak, and A. R. Williams, *Calculated Electronic Properties of Metals* (Pergamon, New York, 1978).
[38] J. L. Perez-Diaz and M. C. Munoz, Phys. Rev. B **50**, 8824 (1994).
[39] J. L. Perez-Diaz and M. C. Munoz, Phys. Rev. B **52**, 2471 (1995).
[40] D. BenDaniel and C. B. Duke, Phys. Rev. **152**, 683 (1966).
[41] P. Harrison, *Quantum Wells, Wires and Dots* (Wiley, New York, 2005).
[42] H. Kroemer and Q. Zhu, J. Vac. Sci. Technol. **21**, 551 (1982).
[43] W. Harrison, J. Appl. Phys. **110**, 113715 (2011).